View metadata, citation and similar papers at core.ac.uk

brought to you by CORE

provided by Explore Bristol Research

Zhang, J., Felice, M., Velichko, A., & Wilcox, P. (2016). Investigation into angular and frequency dependence of scattering matrices of elastodynamic scatterers. In 42nd annual review of progress in quantitative nondestructive evaluation: Incorporating the 6th European-American workshop on reliability of NDE. [040003] (AIP Conference Proceedings; Vol. 1706). American Institute of Physics Inc.. DOI: 10.1063/1.4940497

Publisher's PDF, also known as Version of record

Link to published version (if available):
10.1063/1.4940497

Link to publication record in Explore Bristol Research
PDF-document

This is the final published version of the article (version of record). It first appeared online via American Institute of Physics at http://dx.doi.org/10.1063/1.4940497. Please refer to any applicable terms of use of the publisher.

University of Bristol - Explore Bristol Research

General rights

This document is made available in accordance with publisher policies. Please cite only the published version using the reference above. Full terms of use are available:
http://www.bristol.ac.uk/pure/about/ebr-terms.html

Investigation into angular and frequency dependence of scattering matrices of elastodynamic scatterers

Jie Zhang, Maria Felice, Alexander Velichko, and Paul Wilcox

Citation: AIP Conference Proceedings **1706**, 040003 (2016); doi: 10.1063/1.4940497
View online: http://dx.doi.org/10.1063/1.4940497
View Table of Contents: http://scitation.aip.org/content/aip/proceeding/aipcp/1706?ver=pdfcov
Published by the AIP Publishing

Articles you may be interested in

Frequency and angular dependence of bottom scattering strength in shallow water with a sandy seabed
J. Acoust. Soc. Am. **122**, 3092 (2007); 10.1121/1.2943051

BEM and the use of explicit frequency-dependent matrices—A study on computing wave scattering and radiation
J. Acoust. Soc. Am. **105**, 1287 (1999); 10.1121/1.426138

Frequency-dependent angular scattering of ultrasound by tissue-mimicking materials and excised tissue
J. Acoust. Soc. Am. **80**, 229 (1986); 10.1121/1.394169

Angular Dependence of Raman Scattering Intensity
J. Chem. Phys. **52**, 1584 (1970); 10.1063/1.1673171

Angular Dependence of Nonlinear Light Scattering
J. Chem. Phys. **45**, 3882 (1966); 10.1063/1.1727421

Reuse of AIP Publishing content is subject to the terms at: https://publishing.aip.org/authors/rights-and-permissions IP: 137.222.181.178 On: Tue, 25 Oct 2016 08:41:50

Investigation into Angular and Frequency Dependence of Scattering Matrices of Elastodynamic Scatterers

Jie Zhang[1, a)], Maria Felice[1, 2, b)], Alexander Velichko[1, c)] and Paul Wilcox[1, d)]

[1]*Department of Mechanical Engineering, University Walk, University of Bristol, Bristol BS8 1TR, UK*
[2]*MV Felice is now at the Manufacturing Technology Centre, Ansty Park, Coventry CV7 9JU, UK*

[a)]Corresponding author: j.zhang@bristol.ac.uk
[b)] maria.felice@the-mtc.org, [c)]a.velichko@bristol.ac.uk and [d)]p.wilcox@bristol.ac.uk

Abstract. The scattering behaviour of a finite-sized elastodynamic scatterer in a homogeneous isotropic medium can be encapsulated in a scattering matrix (S-matrix) for each wave mode combination. Each S-matrix is a continuous complex function of 3 variables: incident wave angle, scattered wave angle and frequency. In the paper, the S-matrices for various scatterers (circular holes, straight smooth cracks, rough cracks and 4 circular holes in an area of interest) are investigated. It is shown that, for a given scatterer, the continuous data in the angular dimensions of an S-matrix can be represented to a prescribed level of accuracy by a finite number of complex Fourier coefficients. The finding is that the number of angular orders required to characterise a scatterer is a function of scatterer size and is related to the Nyquist theorem. The variation of scattering behaviour with frequency is examined next and is found to show periodic oscillation with a period which is a function of scatterer size and its geometry. The shortest period of these oscillations indicates the maximum frequency increment required to accurately describe the scattering behaviour in a specific frequency range. Finally, the maximum angular order and frequency increments for the chosen scatterers in a specific frequency range are suggested.

INTRODUCTION

A scattered wave field from a scatterer contains a great deal of information about its geometry and can be mathematically termed as a scattering matrix (S-matrix) [1-2]. For quantitative non-destructive evaluation (NDE) of materials and structures, scattering by scatterers is therefore of great interest in the place for defect detection, classification and characterisation which includes to determine its size, shape and orientation [3]. A thorough understanding of such direct scattering problem is a necessary prerequisite for solving above issues. For example, the solutions of the elastodynamic scattering from a scatterer, either for bulk waves or guided waves, can be used for parametric study of optimising defect inspection configuration in which either conventional single crystal ultrasonic transducers or ultrasonic arrays [4] can be used. The optimised configuration expects to be able to achieve the highest signal to noise ratio (SNR) in either the received signals from conventional single crystal ultrasonic transducers [5] or the reconstructed images from ultrasonic arrays [6] in all possible configurations. The solutions of the elastodynamic scattering from a scatterer are also benefit to defect classification and characterisation which mathematically is the inverse problem of obtaining the defect geometry from the scattered field [7], the examples of which in practice include quantitative damage imaging using minimum sensor density [8], defect characterisation using the experimentally measured scattered signals from an ultrasonic array [1], etc.

42nd Annual Review of Progress in Quantitative Nondestructive Evaluation
AIP Conf. Proc. 1706, 040003-1–040003-9; doi: 10.1063/1.4940497
© 2016 AIP Publishing LLC 978-0-7354-1353-5/$30.00

Reuse of AIP Publishing content is subject to the terms at: https://publishing.aip.org/authors/rights-and-permissions IP: 137.222.181.178 On: Tue, 25 Oct 2016 08:41:50

The work described in the paper is motivated by how to efficiently simulate the scattered ultrasonic signals of a scatterer, especially in ultrasonic array inspection systems. In this case, each either transmitting or receiving element in any array causes waves to be incident or scattered on a particular scatterer from different angles. Therefore in order to simulate the data associated with a scatterer, termed as the full matrix capture (FMC) array data set [9], it is necessary to compute the amplitude and phase of scattered signals over a range of different incident and scattering angles. The efficiency of model execution therefore becomes to significant importance and it is dominated by the minimum number of angle and frequency required for generating S-matrix, apart from choosing an efficient scattering model. The solution of these minimum requirements will also benefit to efficient S-matrix data storage and defect characterisation in NDE applications.

In this paper, the S-matrices of several simulated two-dimensional (2D) embedded scatterers are first theoretically calculated using various scattering models. The angular and frequency dependence of these S-matrices are then analysed. The minimum angular and frequency resolution required to accurately describe these S-matrices are finally given and discussed. Note that only the S-matrices from longitudinal incident and scattered wave modes for 2D scatterers are considered in this paper.

DEFINITION OF S-MATRIX

The interaction between ultrasonic waves and a scatterer can be encoded by its far field S-matrix which is defined as the far field complex amplitude of scattered signals from a scatterer as a function of the incident and scattering angles and frequency [1-2]. When a plane wave of amplitude u_i is incident on a 2D scatterer, a scattered field is generated and in the far field decays in inverse proportion to the square root of the distance from the defect. Note that here a 2D scatterer can be defined by its geometry type and size. If the amplitude of the scattered wave at a distance r is u_s, then the far field S-matrix is given by [1-2],

$$S(f,\alpha,\beta) = \frac{u_s}{u_i}\sqrt{\frac{r}{\lambda}}exp\big(-ik(r-\lambda)\big), \tag{1}$$

where, f is the frequency, λ is the wavelength and k is wave number ($k = 2\pi / \lambda$). For an embedded scatterer, α and β are the incident and scattering angles at the scatterer with respect to the defined lateral axis. The angle definitions are as shown in Figure 1, where the coordinate origin lies at the nominal center of the scatterer.

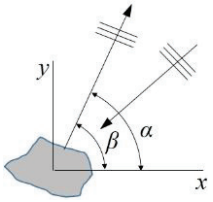

FIGURE 1. Schematic of geometry showing scatterer, axes and wave angle definitions.

For a specific frequency, the S-matrix can be written as a 2D Fourier series,

$$S(\alpha,\beta) = \sum_{m=-\infty}^{m=+\infty}\sum_{n=-\infty}^{n=+\infty} A(m,n)exp\big(i(m\alpha + n\beta)\big), \tag{2}$$

with complex Fourier coefficient $A(m,n)$, where m and n represent as the incident and scattering angular orders respectively. In practice, $A(m,n)$ can be obtained using 2D fast Fourier transform (2D-FFT) for S respect to α and β.

SIMULATED S-MATRICES

In order to investigate the scattering behaviour of general embedded scatterers, 4 different type of scatterers are chosen and they are as shown in Figures 2(a)-(d) which include circle hole, straight crack, rough crack and 4 circular holes in an area of interest. Here an embedded scatterer means that it is remote from any edges of a structure. In each figure, a dashed circle is used to restrict the largest distance between the discretised points on the profile of each scatterer. This circle has a radius of a/2 where a is defined as the scatterer size. Note that the center of a dashed circle is the nominal center of a scatterer and its location is defined as the scatterer location in a modelled 2D structure [6].

Reuse of AIP Publishing content is subject to the terms at: https://publishing.aip.org/authors/rights-and-permissions IP: 137.222.181.178 On: Tue, 25 Oct 2016 08:41:50

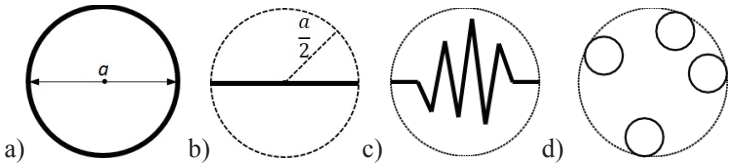

FIGURE 2. The geometry of a modelled; (a) circular hole, (b) straight crack, (c) rough crack (d) 4 circular holes in an area of interest. Note that (a,b,c,d) is labelled as scatterer geometry types 1-4 respectively.

Note that for the crack types, as shown in Figures 2 (b) – (c), the scatterer center is at the middle of the straight line defined by the two points on the circle. In order to easily describe scatterer type, the scatterers with a geometry as shown in Figures 2(a-d) are labelled as scatterer geometry types 1-4 respectively. These scatterers are assumed in homogeneous isotropic Aluminium with a density of 2700 kg/m^3, a Young's modulus of 71 GPa, a Possion's ratio of 0.34 and hence a wave speed, c = 6400 m/s. Note that in the benchmark S-matrix calculation the incident and scattering angles range from 0° to 360° with an angular increment of 1°.

The exact analytical scattering solutions of circular hole [10] and straight crack [11] exist and they can be used to calculate the benchmark S-matrices of these scatterers. However, there is no exact scattering solutions available for the other chosen scatterer types. Instead, a local finite element (FE) model which uses non-reflecting boundary condition and no absorbing regions [12] is used. In this way, the S-matrices of the chosen scatterers with any sizes can be efficiently calculated. It should be noted that, for a scatterer with a specific geometry type, its S-matrix is a function of incident angle, scattering angle and the ratio of scatterer size to wavelength which is equivalent to frequency, i.e., α, β and a/λ. As examples, Figures 3-4 compare the moduli of the S-matrices for the chosen scatterers with a size of $a = 0.015\lambda$ and $a = 10\lambda$. In Figures 3(a-b) and 4(a-b), the diagonal ridges that run along the straight lines $|\alpha - \beta| = 180°$ correspond to the shadowing effect in the forward-scattered direction. The diagonal ridges run along the straight lines $\alpha + \beta = 180°$ and $\alpha + \beta = 540°$ indicate the specular scattering in the backward-scattered direction. Comparing Figures 3-4 for a same geometry type, it can be seen that the smaller scatterer exhibits a reduced overall maximum scattering coefficient relative to the larger scatterer as well as more uniform scattered amplitudes over a wider range of angles. Also it can be seen that for the cracks with a same size, the segment surfaces on the cracks can smear out the scattering energy, especially in the back-scattered direction, and this can either reduce or increase the overall maximum scattering coefficient in the S-matrices [13].

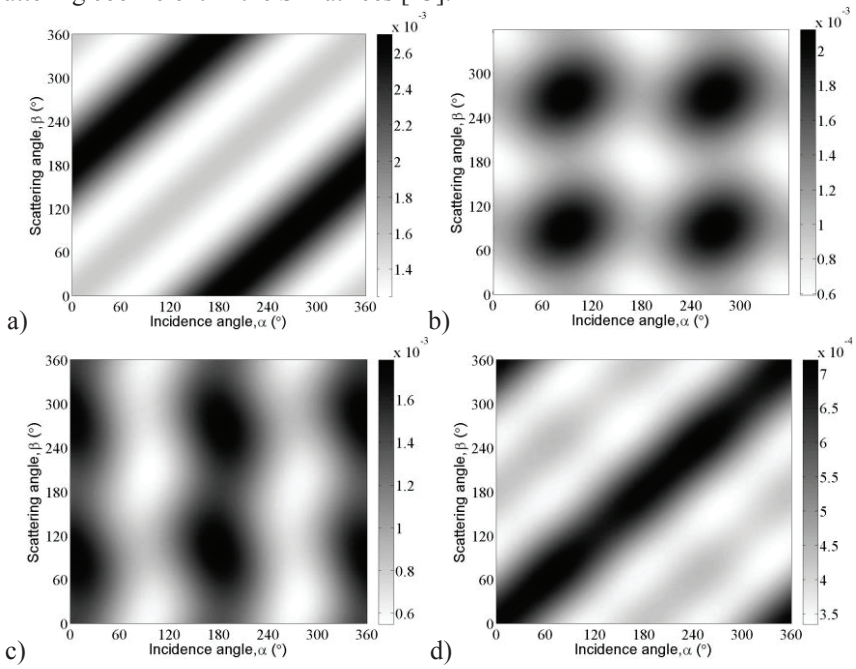

FIGURE 3. Modulus of S-matrix of a scatter with a size of $a = 0.015\lambda$ and geometry type; (a-d) 1-4. Note that the grey-scale is linear.

Reuse of AIP Publishing content is subject to the terms at: https://publishing.aip.org/authors/rights-and-permissions IP: 137.222.181.178 On: Tue, 25 Oct 2016 08:41:50

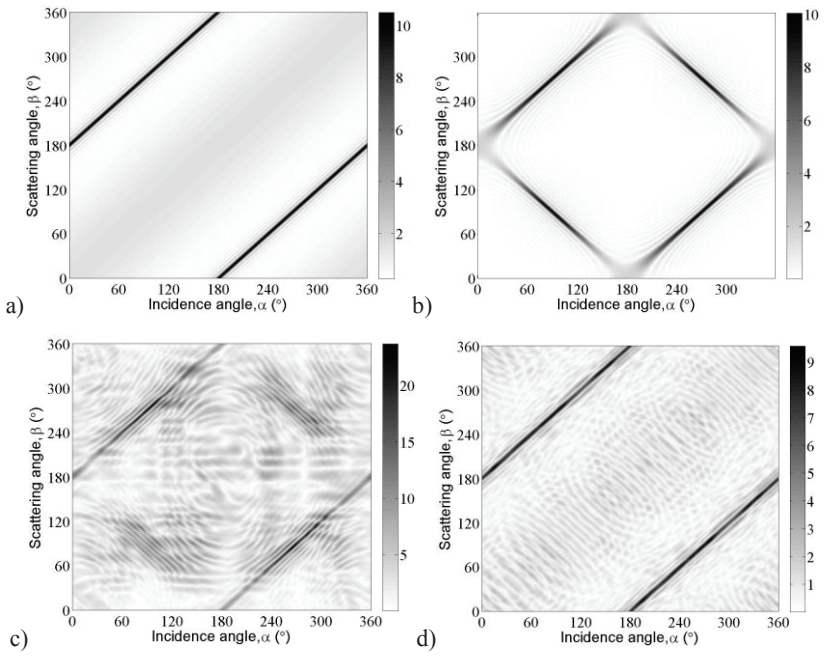

FIGURE 4. Modulus of S-matrix of a scatter with a size of $a = 10\lambda$ and geometry type; (a-d) 1-4.

ANGULAR DEPENDENCE OF S-MATRIX

It should be noted that in the angular dimensions of S-matrix, the data can be equivalently represented by the complex coefficients of its 2D Fourier series, the modules of which, $|A(m,n)|$, for the S-matrices in Figures 3-4, are as shown in Figures 5-6. In each figure, each of Fourier series corresponds to a different angular order. Comparing Figures 3-6 for the scatterers with a same size but different geometry type, it can be seen that, although these S-matrices have different shapes their Fourier coefficients have the similar maximum angular orders for Fourier coefficients with amplitudes above a defined amplitude threshold.

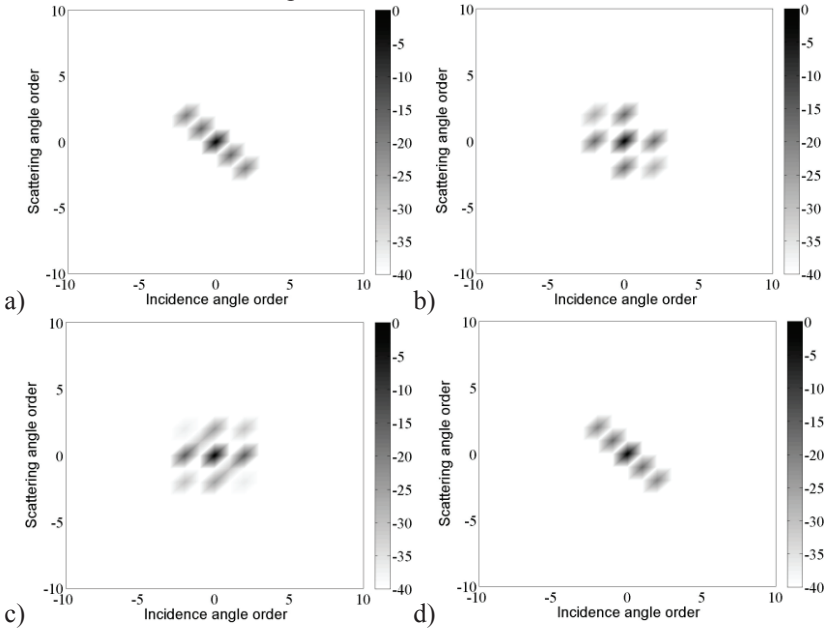

FIGURE 5. Modulus of Fourier coefficients of Figures 3; (a-d) (a-d). Note that these scatterers have a size of $a = 0.015\lambda$. The grey scale is decibels relative to the largest coefficient in each case.

Reuse of AIP Publishing content is subject to the terms at: https://publishing.aip.org/authors/rights-and-permissions IP: 137.222.181.178 On: Tue, 25 Oct 2016 08:41:50

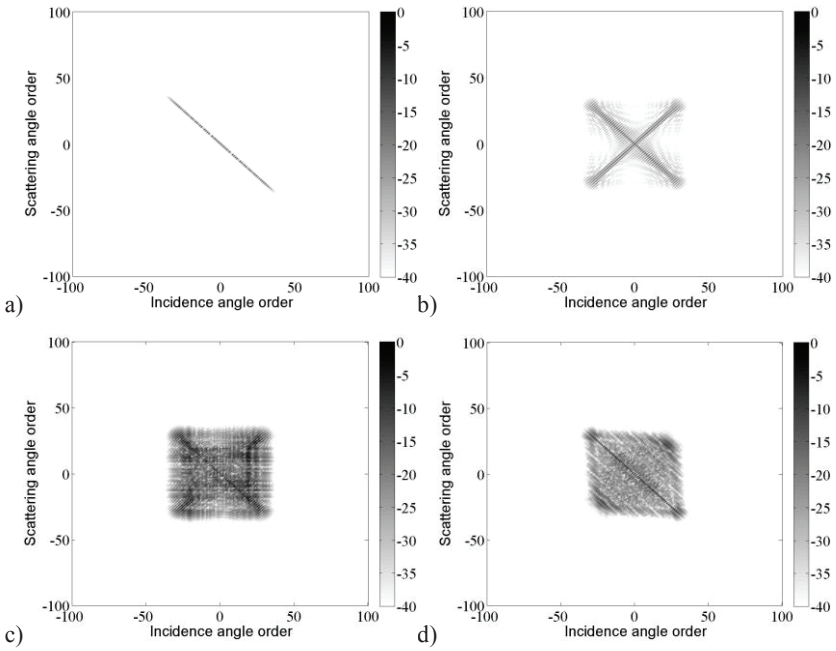

FIGURE 6. Modulus of Fourier coefficients of Figures 4; (a-d) (a-d). Note that these scatterers have a size of $a = 10\lambda$. The grey scale is decibels relative to the largest coefficient in each case.

For example, for the scatterers with a size of $a = 10\lambda$ as shown in Figure 6, the maximum angular order is $N = 37$ for both incident and scattering angles under an amplitude threshold of -40dB. This in turn implies that, for these scatterers, the S-matrice need to be computed at just $2N + 1 = 75$ intervals between 0 and 360° in order to encapsulate all the information to a -40 dB level of accuracy. Comparing Figures 5-6, it is also observed that a larger scatterer require a smaller angular interval.

In order to work out a general angular sampling rule in S-matrix calculation, a large population of S-matrices for the scatterers with the geometry types 1-4, as shown in Figure 2, and the sizes ranging from 0.015λ - 20λ with an increment of 0.015λ is first simulated. The maximum angular order of each simulated S-matrix is then extract under the amplitude threshold of -40 dB. As an example, Figure 7(a) show the variation of maximum angular order of Fourier coefficient, N, with the amplitude threshold of -40dB as a function of scatterer size, a/λ, for the chosen scatterers. As shown, the maximum angular order of Fourier coefficient starts at $(3, 0.015\lambda)$ which is extracted from Figure 5 and then monotonically increases with scatterer size. This variation indicates the dynamic range used to determine the maximum order of Fourier coefficient required. As shown, the trend is approximately linear with scatterer size and suggests that the number of angular orders required to characterise a scatterer of a given size can be readily estimated.

According to the Nyquist criterion, for a cylindrical scattering object with a diameter of a, the minimum number of angular observation required to decode its scattered field is $2\pi a/\lambda$ [8]. This corresponds to the angular order of $\pi a/\lambda - 0.5$ and this corresponds the solid straight line as shown in Figure 7(a). Also shown in Figure 7(a) is the dashed line obtained from fitting the data by,

$$N_f = \frac{k_f \pi a}{\lambda} + N_m \tag{3}$$

where k_f and N_m is the gradient and intercept of the fitted line respectively. Note that for the dashed line in Figure 7(a) N_m corresponds to the maximum required angular order for the minimum size scatterers, i.e., $N_m = 3$ when $a = 0.015\lambda$ and $k_f = 1.1$. From Figure 7(a) it can be seen that the solid line obtained from the Nyquist criterion defines the lowest angular order requirement and the actual requirement could be higher in practice depending on the required amplitude accuracy level.

Using $\Delta\alpha = 360/(2N - 1)$, Figure 7(b) shows the corresponding angular intervals as a function of scatterer size. Again in Figure 7(b) it is shown that the angular increment does not depend on the geometry shape of scatterers but only on their overall size and this is related to the Nyquist criterion. Also shown in Figure 7(b) is that the maximum angular required to guarantee the accuracy better than -40 dB is smaller than that obtained according to the Nyquist criterion.

Reuse of AIP Publishing content is subject to the terms at: https://publishing.aip.org/authors/rights-and-permissions IP: 137.222.181.178 On: Tue, 25 Oct 2016 08:41:50

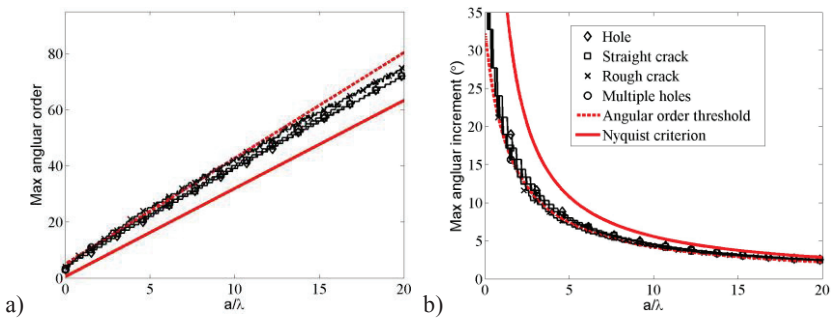

FIGURE 7. Results for angular sampling control of Fourier coefficient of S-matrix as a function of scatterer size for; (a) maximum angular order and (b) maximum angular increment.

FREQUENCY DEPENDENCE OF S-MATRIX

The simulated S-matrices in the previous section, i.e., for the scatterers with sizes ranging from $a = 0$ - 20λ and a size increment of 0.015λ at a given frequency, are equivalent to, for a given scatterer size of a, frequency variation from $f = 0 – 20$ c/a with an increment of $\Delta f = 0.015$ c/a. For example, if the size of a scatterer is $a = 4$ mm and $c =$ 6400 m/s, the frequencies range from 0 to 32 MHz with an increment of 24.5 kHz. These data are used in this section to investigate the oscillation period of scattering coefficient and set frequency increment required in S-matrix calculation.

Figures 8(a-d) compare the real parts of the scattering coefficient at various incident and scattering angles, α and β, from the chosen scatterers as a function of frequency (equivalent to the ratio between wave speed and defect size, c/a) and they show periodic oscillations. In Figure 8(b) $\alpha = \beta = 180°$ and $\alpha = \beta = 90°$ in the other figures. Note that these chosen examples represent relative high frequency oscillation behaviour of the S-matrix from each scatterer. Figure 9 shows the Fourier transform spectrum of each figure in Figure 8. The location of peak amplitude in Figure 9 is the oscillation frequency, f_o, and related to the oscillation period of the scattering coefficient, T_o, in Figure 8.

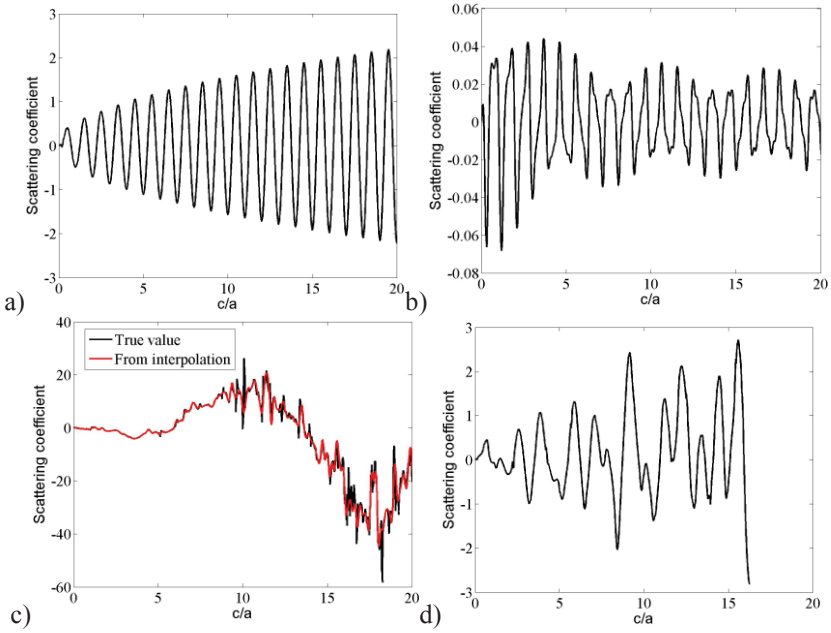

FIGURE 8. Examples of the oscillation behavior of the real part of the scattering coefficients with frequency (equivalent to the ration between wave speed and defect size, c/a) for the scatterer with a geometry type; (a-d) 1-4.

Reuse of AIP Publishing content is subject to the terms at: https://publishing.aip.org/authors/rights-and-permissions IP: 137.222.181.178 On: Tue, 25 Oct 2016 08:41:50

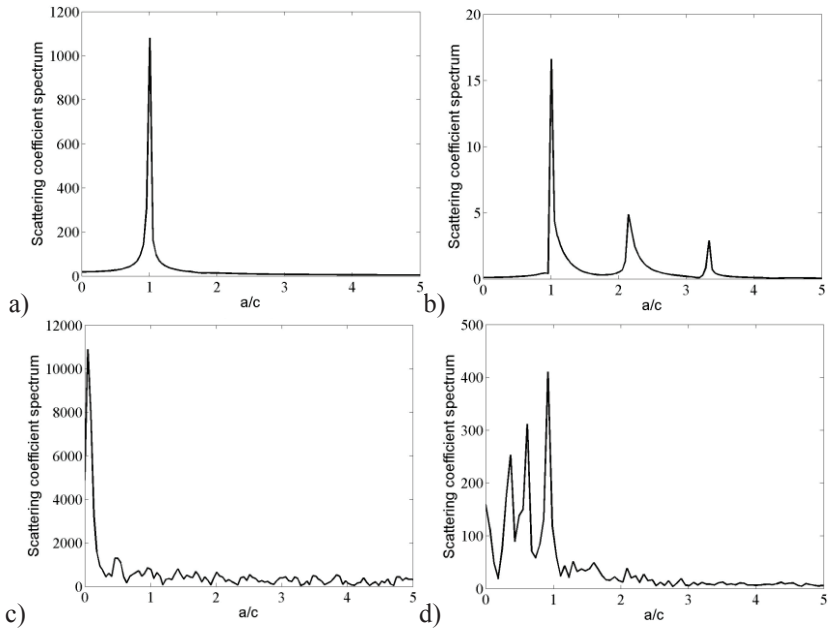

FIGURE 9. Fourier transform spectrum of Figure 8; (a-d) (a-d).

As shown in Figures 8-9, the oscillation behaviors are different; the circular hole has a single oscillation frequency, $f_o = a/c$, the straight crack has 3 different oscillation frequencies with the first one at $f_o = a/c$, the rough crack shows a strong direct current value and multiple oscillation frequencies across a wide range up to $f_o = 5a/c$ and the 4 circular holes in an area of interest has 3 main oscillation frequencies within $f_o \leq a/c$.

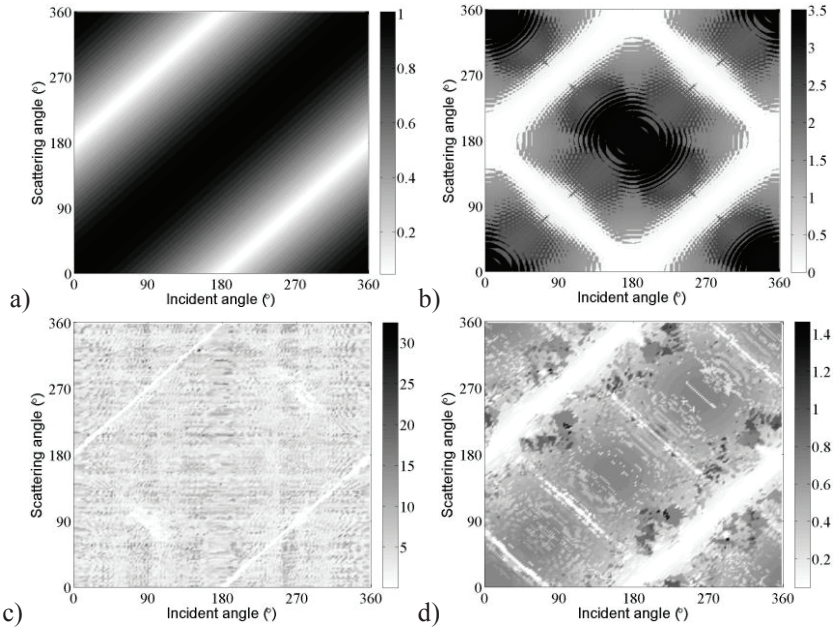

FIGURE 10. Maximum oscillation frequency with the scattering Fourier amplitude above -20 dB of the maximum at each incident and scattering angle combination for the scatterer with a geometry type; (a-d) 1-4.

The same procedure was repeated to investigate the oscillation behavior of scattering coefficient at each incident and scattering angle combination for all chosen scatterers. The oscillation frequencies with an amplitude above -20 dB of the maximum are extracted and they are shown in Figure 10. From Figure10, it can be seen that high oscillation

Reuse of AIP Publishing content is subject to the terms at: https://publishing.aip.org/authors/rights-and-permissions IP: 137.222.181.178 On: Tue, 25 Oct 2016 08:41:50

frequency happens at the area around $\alpha = \beta = 180°$, especially for the cracks. It can be also seen that comparing with the other scatters, the rough crack has a wide range of oscillation frequencies.

Considering a cosine signal with a period of T and N_c ($N_c > 100$) number of points, the question of sampling is what the minimum number of sampling point, N_e, is required to reconstruct the actual signal with a defined accuracy level using a linear interpolation process. Here, the measurement accuracy level is indicated by the root mean square (RMS) error by [14],

$$e_e(N_e) = \frac{\sqrt{\frac{1}{N_c}\sum_{n=0}^{N_c-1}\left[g\left(\frac{nT}{N_c-1}\right)-g_c\left(N_e,\frac{nT}{N_c-1}\right)\right]^2}}{\sqrt{\frac{1}{N_c}\sum_{n=0}^{N_c-1}\left[g\left(\frac{nT}{N_c-1}\right)\right]^2}} \times 100\%, \tag{4}$$

where, $g_c\left(N_e,\frac{nT}{N_c-1}\right)$ is the signal amplitude obtained using an interpolation method based on N_e number of evenly distributed sampling points. It should be noted that all N_c number of points can be accurately estimated using an interpolation method when N_e is large enough [14]. A general rule is that 8 sampling points in a cycle can ensure the RMS error of the spline interpolation method less than 1% [14]. Considering this sampling rule together with the maximum oscillation frequency in Figure 10, the frequency sampling required should be 8 sampling points per cycle for the shortest period and this can ensure the RMS error of calculated S-matrix using the spline interpolation method less than 1%.

DISCUSSION

In a conservative way, the maximum angular increments required for all chosen scatterers can be calculated using equation 3 with k_f=1.1 and N_m = 3 and they are listed in Table 1. In this way, a S-matrix with the angular increment of $\Delta\alpha_m$, listed in Table 1, dcan be calculated first, and then the S-matrix with a fine angular increment, e.g., 1°, can be obtained using the Fourier linear interpolation (equation 2). The accuracy of the resultant S-matrix can be examined by the RMS error,

$$e_\alpha(\Delta\alpha_m, f) = \frac{\sqrt{\frac{1}{4\pi^2}\int_0^{2\pi}\int_0^{2\pi}[|S_F(\Delta\alpha_m,f,\alpha,\beta)|-|S_B(f,\alpha,\beta)|]^2 d\alpha d\beta}}{\frac{1}{4\pi^2}\int_0^{2\pi}\int_0^{2\pi}|S_B(f,\alpha,\beta)|d\alpha d\beta} \times 100\%, \tag{5}$$

where, S_B is the benchmark S-matrix obtained directly from the scattering model and using the angular increment of 1° and S_F is the measured S-matrix obtained using the Fourier linear interpolation on the S-matrix with the angular increment of $\Delta\alpha_m$. The measured error $e_\alpha \leq 1\%$ for all chosen scatterers and this validates the proposed angular sampling rule.

TABLE 1. Angular and frequency increments required to make sure $e_\alpha \leq 1\%$ and $e_f \leq 1\%$ in the range of $0 < a \leq 20\lambda$.

Defect type	Circular hole	Straight crack	Rough crack	Multiple circular holes
Angular increment, $\Delta\alpha$ (°)	$360/(2.2\,\pi a/\lambda + 5)$			
Shortest period, T_m (c/a)	1	0.29	0.13	0.71
Frequency increment, $\Delta f_m = T_m/7$ (c/a)	0.14	0.04	0.02	0.1

The similar process can also be used for examining the angular increment requirement. The level of accuracy of the calculated S-matrix using the linear spline interpolation can be indicated by the mean amplitude error between the measured results, S_I, and the true values, S_B, across the whole frequency range, i.e.,

$$e_f(\Delta f_m, \alpha, \beta) = \frac{\sqrt{\frac{1}{N_f}\sum_f[\mathcal{F}(S_I(\Delta f,f,\alpha,\beta))-\mathcal{F}(S_B(f,\alpha,\beta))]^2}}{\frac{1}{N_f}\sum_f|\mathcal{F}(S_B(f,\alpha,\beta))|} \times 100\%, \tag{6}$$

where, $\mathcal{F}$ is an operator to get either real and imaginary parts of a S-matrix, Δf_m is the frequency increment of the sampling points and N_f is the total number of frequency. As an example, Figure 8(c) compares the scattering coefficients from the benchmark S-matrix (black curve) and the one from the spline interpolation process (red curve). As shown, their difference is negligible. Based on all benchmark S-matrices for a given type of scatterer and the maximum frequency increments required listed in Table 1, e_f for all chosen scatterers are calculated and it is shown

Reuse of AIP Publishing content is subject to the terms at: https://publishing.aip.org/authors/rights-and-permissions IP: 137.222.181.178 On: Tue, 25 Oct 2016 08:41:50

that $e_f \leq 1\%$. This means that Table 1 can be used to chosen the angular and frequency increments in S-matrix computation for array FMC data generation with the accuracy of $e_\alpha \leq 1\%$ and $e_f \leq 1\%$.

SUMMARY

The angular and frequency dependency of scattering matrices of the chosen scatterers are investigated and the general guide of how to choose maximum angular and frequency increments for either FMC array data simulation or experimentally characterising defect is suggested. It is shown that the maximum angular increment required to accurately and efficiently describe the scattered wave is a function of scatterer size to wavelength ratio and does not depend scatterer geometry. However, the maximum frequency increment required is dependent on both scatterer size and the complexity of scatterer geometry.

The practical consequence of the findings of the angular and frequency dependency of the S-matrix can lead to efficient array data simulation and efficient experimental inspection. For example, the computation cost of generating the S-matrices can be reduced and this leads to efficient array data simulation using the forward model [6]. The reduced size of the S-matrix also benefits to data storage and efficient defect characterisation. For example, the findings can help to design sparse array configuration with minimum number of sensors for experimental defect characterisation using either bulk waves or guided waves.

ACKNOWLEDGMENTS

This work was supported through the technology transfer project within the UK Research Centre in NDE (RCNDE) funded by EPRSC (grant number EP/L022125/1).

REFERENCES

1. J. Zhang, B. Drinkwater, and P. Wilcox, IEEE Trans. Ultrason. Ferr. Freq. Contr. **55**, 2254-2265, (2008).
2. L. W. Schmerr, *Fundamentals of ultrasonic nondestructive evaluation - a modeling approach* (Prenum press, New York, 1998), pp. 305-371.
3. J. D. Achenbash, A. K. Gautesen and H. McMaken, *Ray methods for waves in elastic solids* (Pitman Advanced Publishing Program, Boston, 1992), pp. 1-9.
4. B. W. Drinkwater and P. D. Wilcox, NDT Int. **39**, 525-541, (2006).
5. D. N. Alleyne and P. Cawley, NDT Int. **25**, 11-22, (1992).
6. J. Zhang, B. W. Drinkwater, P. D. Wilcox, and A. Hunter, NDT Int. **43**, 123-133, (2010).
7. D. Colton, J. Coyle and P. Monk, SIAM Rev. **42**, 369-414, (2000).
8. C. H. Wang and L. R. F. Rose, "Minimum sensor density for quantitative damage imaging", in proceedings of the 9th international workshop on structural health monitoring, edited by Fu-Kuo Chang (Dohrmann Grove, Stanford University, CA, USA, 2013), pp. 2248-2255.
9. C. Holmes, B. W. Drinkwater and P. D. Wilcox, NDT Int. 701-711, (2005).
10. A. L. Lopez-Sanchez, H. Kim, L. W. Schmerr Jr., and A. Sedov, J. Nondestruct. Eval. **24**, 83-96, (2005).
11. E. Glushkov, N. Gluskova, A. Ekhlakov and E. Shapar, Wave Motion, **43**, 458-473, (2006).
12. A. Velichko and P. Wilcox, J. Acous. Soc. Am. **128**, 1004-1014, (2010).
13. J. Zhang, B. Drinkwater, and P. Wilcox, IEEE Trans. Ultrason. Ferr. Freq. Contr. **58**, 2163-2171, (2011).
14. F. R. Moore, Comput. Music J. **1**, 26-29, (1977).

Reuse of AIP Publishing content is subject to the terms at: https://publishing.aip.org/authors/rights-and-permissions IP: 137.222.181.178 On: Tue, 25 Oct 2016 08:41:50